Inversionless lasing with self-generated driving field

Alexey Belyanin,[1,2] Cleo Bentley,[3] Federico Capasso,[1,4] Olga Kocharovskaya,[1,2] and Marlan O. Scully[1,5]
[1]*Physics Department and Institute for Quantum Studies, Texas A&M University, College Station, Texas 77843*
[2]*Institute of Applied Physics, Russian Academy of Science, 46 Ulyanov Street, 603600 Nizhny Novgorod, Russia*
[3]*Department of Physics, Prairie View A&M University, Prairie View, Texas 77446*
[4]*Bell Laboratories, Lucent Technologies, 600 Mountain Avenue, Murray Hill, New Jersey 07974*
[5]*Max-Planck-Institut für Quantenoptik, 85748 Garching, Germany*
(Received 2 January 2001; published 12 June 2001)

We propose and study resonant ladder schemes of inversionless lasing on a fast-decaying transition when the population inversion is not possible or very difficult to achieve. The driving field on a neighboring, slowly decaying transition is not imposed externally, but is self generated in the same active medium. Inversionless lasing in such schemes avoids the problem of driving-field absorption and leads to considerable reduction in the required pumping rate. Applications of such schemes include inversionless ultraviolet and soft x-ray lasing in gas lasers and inversionless generation of coherent mid/far-infrared emission on intersubband (interlevel) transitions in multiple quantum-well or quantum-dot laser diodes.

DOI: 10.1103/PhysRevA.64.013814 PACS number(s): 42.50.Gy, 42.55.Ah, 42.55.Px, 42.55.Vc

I. INTRODUCTION

Amplification and lasing without inversion (LWI) is a current research topic in quantum electronics. The basic idea is that quantum coherence created in the medium by means of a strong driving field helps to partially eliminate resonant absorption on the transition of interest and to achieve gain without population inversion on this transition. This subject has been intensively investigated both theoretically and experimentally; see Ref. [1] for reviews.

Now, after a series of proof-of-principle experiments, the time is ripe for studying specific systems where the implementation of LWI could be of real help. It is clear that LWI could be particularly useful in situations where population inversion is difficult to maintain due to, e.g., ultrafast relaxation on the operating transitions or inefficient pumping. The obvious examples are high frequency ultraviolet (UV), x-ray and gamma-ray lasers [2], and semiconductor mid/far-infrared lasers based on intersubband transitions [3]. Another promising application of quantum coherence ideas is efficient frequency up or down conversion and other nonlinear optical processes [4]. A related field of research is producing transparent high-refractive index media, e.g., for microlithography applications [5].

So far, efforts in the above directions were mainly restricted to the case of *external* driving fields imposed on the active medium and to the schemes where inversion is absent not only on the operating but also on the driven transition. Work where the drive was intracavity generated appears in the recent paper [6], where dual-wavelength lasing in the ladder and *V*-schemes were considered with application to optical transitions in Ba and Rb atoms in a vapor cell.

However, in many cases, external driving gives rise to difficulties that can become unsurmountable. For example, in order to achieve high intensities of generated fields, or high refractive index, one has to use dense active media: dense gases or even solids. This can often lead to problems with drive absorption and reflection, transverse inhomogeneity, or overlap of drive and probe beams. Examples include semiconductors and very dense gases where the driving by external laser radiation is questionable. Besides, in semiconductors the use of external lasers for driving, pumping, or frequency conversion is impractical; electric current pumping is required for practical applications.

Schemes with external driving encounter substantial difficulties in the frequency up-conversion regime, when the copropagating geometry of the drive and probe field is realized. In this case the absorption length for the drive field is inevitably much shorter than the amplification length for the probe field [7–9]. This follows from the requirement of fast relaxation on the driving transition, as compared to probe transition, which is inherent in such schemes. Note that there were several suggestions on how to get rid of this unfavorable ratio of relaxation times in the most popular *V* and Λ schemes, with or without inversion on the driving transition [7–9]. In Ref. [8], inversionless lasing on the fast-decaying transition in V and Λ schemes was analyzed. It was found that the net gain is possible when the populations on the drive transition are inverted *and* the drive or probe fields are detuned from one-photon resonance. In this case, the inversionless gain contains inevitably the large detuning factor in the denominator. The potential advantage of ladder schemes with slowly decaying drive transition is that the maximum gain for the probe field on the fast-decaying transition is achieved exactly on resonance; see below. In Refs. [7,9] it was shown that inversionless lasing on the fast-decaying transition in the *V* configuration can be achieved when both drive and probe fields are detuned from corresponding atomic transitions but maintain two-photon resonance. It was found that under the conditions of a strong inhomogeneous broadening, the maximum gain in the detuned case can be even higher than for the resonant driving. The price one has to pay is Raman inversion for the substantial amount of atoms within an inhomogeneously broadened line. Only the groups of atoms strongly driven by the drive field (with transition frequencies close enough to the two-photon resonance) do not have Raman inversion. Our analysis for the ladder scheme described in Sec. IV yields the same result. More-

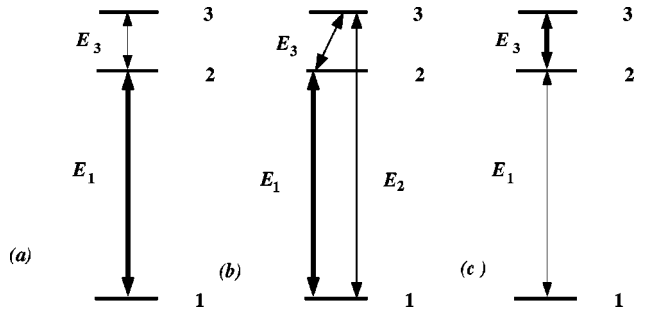

FIG. 1. The simplest schemes of inversionless lasing with a self-generated driving-field. (a) and (b) Lower ladder scheme: strong driving-field E_1 is generated on the $2\rightarrow1$ transition giving rise to excitation of weak (a) monochromatic and (b) bichromatic lasing mode. (c) Upper ladder scheme: strong field E_3 on the $3\rightarrow2$ transition leads to inversionless generation of field E_1.

over, the requirement to incoherent pump is such that in the absence of a drive field, it produces the Raman inversion for all atoms within the inhomogeneous line.

In this paper, we study two types of resonant ladder schemes [Figs. 1(a-c)], labeled lower [Fig. 1(a,b)] and upper level [Fig. 1(c)] ladder schemes according to the position of the driving field, in which the driving field is not imposed externally, but is self generated in the same active medium. In other words, the system is a usual laser (with population inversion) on one transition (drive transition), and inversionless laser with respect to generation on another transition (probe transition). The goal is to get inversionless lasing on the fastest-decaying transition where it is difficult [scheme in Fig. 1(c)] or impossible [scheme in Figs. 1(a,b)] to provide population inversion. LWI becomes possible due to the coherent driving field generated on the neighboring, inverted transition. The inversion is easily achievable due to the slow decay on this transition. In such schemes, the problem of drive absorption is completely eliminated since the relaxation of populations on the drive transition is much slower than on the probe transition.

LWI in ladder schemes has been studied in a number of works; see, e.g., [6,10–12]. However, to our knowledge, the specific case of LWI on a fast-decaying transition with self-generated drive on a slowly decaying transition, which seems to be the most natural and promising from the practical point of view, has not been analyzed so far.

The most evident application of the schemes shown in Figs. 1(a,b) is quantum-well and quantum-dot semiconductor lasers, where the optical lasing on the interband transition $(2\rightarrow1)$ can be easily excited by injection current pumping, while mid- and far-infrared (IR) generation on the intersubband transition $(3\rightarrow2)$ encounters substantial difficulties.

Basically, there are two major problems. The first one is strong nonresonant losses of the IR field due to free-carrier absorption and diffraction, which become increasingly important at longer wavelengths. The second problem is difficulty in providing population inversion and high enough gain on intersubband transitions to reach threshold of laser action. The intersubband lifetime of excited states is of order 5–10 ps for quantum dots (QD's) and 1 ps for quantum wells (QW's). There were many suggestions to solve these problems by rapid depletion of the lower-lasing state using, e.g., the resonant tunneling to adjacent semiconductor layers [13], transition to yet lower subbands due to phonon emission or even stimulated interband recombination [14,15]; see Refs. [16,17] for a recent review. The successful culmination of these studies was the realization of quantum cascade lasers [18], in which the lower-lasing state is depopulated either by interminiband transport in the superlattice or due to transitions to a lower-lying level separated from the final state of the laser transition by nearly the energy of LO-phonon; see, e.g., Ref. [19] and references therein.

We show in Sec. III that interband lasing on the 1-2 transition in Figs. 1(a,b) allows one to achieve inversionless generation on the 2-3 transition for the ratio of relaxation rates $r_{32}/r_{21}\gg1$, when the inversion between states 3 and 2 cannot be reached for any pumping rates r_{13}. Another possible application of the lower ladder scheme is UV generation in rare-earth ion-doped crystals. Here, a self-generated drive can be rather easily excited on the forbidden f-f transition (this is actually the way that most IR rare-earth lasers work), while UV radiation at the electric dipole allowed, fast decaying transition between a f state and a higher-lying d state can be generated without inversion.

An appealing application of the upper ladder scheme in Fig. 1(c) could be inversionless lasing on the electric dipole-allowed UV 2-1 transition where fast radiative decay makes the realization of population inversion a difficult task. At the same time, population inversion on a slowly decaying 3-2 transition can be rather easily achieved. With respect to lasing on the 3-2 transition, this is in fact a standard four-level laser scheme, widely employed in many solid-state and gas lasers. Here we assume that the incoherent pumping populates some upper level 4, and the subsequent incoherent relaxation from level 4 to level 3 proceeds much faster than all other timescales, so that only three levels can be considered.

It is important to note that in all of the above cases, the long-lived coherence is not required for inversionless generation. It is this fact that makes such schemes viable for semiconductors and high-frequency lasers where the dephasing times are extremely short.

Note that in two other popular configurations, Λ and V schemes, self-generated drive and associated inversion on the drive transition lead to additional absorption instead of excitation near the line center. In this case, inversionless gain could be possible only far from the resonance. Hence, resonant ladder schemes are in fact the only three-level configurations in which inversionless lasing with a self-generating driving field is efficient.

II. BASIC EQUATIONS

Our analysis is based on coupled density-matrix equations and Maxwell equations. For the reader's convenience, we present this basic set of well-known equations that are valid for all three types of schemes in Fig. 1 (see also Ref. [20] specifically for the QW and QD cases). We represent all fields as a series over the corresponding orthonormal set of cavity modes $\mathbf{F}_\lambda$ and introduce slowly varying complex amplitudes of fields and polarizations. For example, we write

$$\mathbf{E}_1(\mathbf{r},t)=\sum_{\lambda}\frac{1}{2}\mathcal{E}_1(t)\mathbf{F}_{1\lambda}(\mathbf{r})\exp(-i\omega_{c1}t)+\text{c.c.} \quad (1)$$

for the field on a $2\rightarrow1$ transition, and the same representations for the fields $\mathbf{E}_{2,3}$ on other transitions.

For each field, we define the complex Rabi frequency $e(t)=d\mathcal{E}(t)/2\hbar$ and write the corresponding wave equation for a given mode:

$$\frac{de_1}{dt}+\kappa_1 e_1=\frac{2\pi i\omega_{c1}d_1^2N}{\hbar n_1^2}\int_{V_c}\sum_j \sigma_{21}^j F_{1\lambda}(\mathbf{r})\ d\mathbf{r}, \quad (2)$$

$$\frac{de_2}{dt}+\kappa_2 e_2=\frac{2\pi i\omega_{c2}d_2^2N}{\hbar n_2^2}\int_{V_c}\sum_j \sigma_{31}^j F_{2\lambda}(\mathbf{r})\ d\mathbf{r}, \quad (3)$$

$$\frac{de_3}{dt}+\kappa_3 e_3=\frac{2\pi i\omega_{c3}d_3^2N}{\hbar n_3^2}\int_{V_c}\sum_j \sigma_{32}^j F_{3\lambda}(\mathbf{r})\ d\mathbf{r}. \quad (4)$$

Here, $d_{1,2,3}$ are the dipole moments of the corresponding transitions, N the total volume density of dipole oscillators in the active region, $\omega_{c1,2,3}$ the frequencies of the cavity modes with refractive indices $n_{1,2,3}$, $\kappa_{1,2,3}$ the cavity losses, and V_c the cavity volume. The variables σ_{21}^j, σ_{31}^j, σ_{32}^j are the slowly varying amplitudes of the corresponding elements of the density matrix, index j labels different electron states contributing to the inhomogeneously broadened line. For a gaseous medium, j denotes different velocity states in the Maxwell distribution. In a system of QD's, j is the dot label. In QW's, index j labels different $\mathbf{k}_\parallel$ states with respect to longitudinal quasimomentum lying in the growth plane.

The functions σ_{ik} are to be found from the density-matrix equations

$$d\sigma_{21}/dt+\Gamma_{21}\sigma_{21}=ie_1n_{12}-ie_2\sigma_{32}^*+ie_3^*\sigma_{31}, \quad (5)$$

$$d\sigma_{31}/dt+\Gamma_{31}\sigma_{31}=ie_2n_{13}-ie_1\sigma_{32}+ie_3\sigma_{21}, \quad (6)$$

$$d\sigma_{32}/dt+\Gamma_{32}\sigma_{32}=ie_3n_{23}-ie_1^*\sigma_{31}+ie_2\sigma_{21}^*, \quad (7)$$

where $n_{ik}=\rho_{ii}-\rho_{kk}$,

$$\Gamma_{21}=\gamma_{21}+i(\omega_{21}+\delta_j-\omega_{c1}),$$

$$\Gamma_{31}=\gamma_{31}+i(\omega_{31}+\delta_j-\omega_{c2}), \quad (8)$$

$$\Gamma_{32}=\gamma_{32}+i(\omega_{32}+\delta_j-\omega_{c3}).$$

Here, the index j was omitted to shorten notations. The quantity δ_j is the difference between the transition frequency for a given jth state and the central frequency ω_{21}, ω_{31}, or ω_{32}.

In atomic media and, under certain approximations, in semiconductors, the density-matrix equations for populations ρ_{ii}, $i=1,2,3$ can be written as

$$d\rho_{11}/dt=-2\,\mathrm{Im}[e_1^*\sigma_{21}]-2\,\mathrm{Im}[e_2^*\sigma_{31}]+r_{21}\rho_{22}+r_{31}\rho_{33}-r_{13}\rho_{11},$$

$$d\rho_{22}/dt=2\,\mathrm{Im}[e_1^*\sigma_{21}]-2\,\mathrm{Im}[e_3^*\sigma_{32}]+r_{32}\rho_{33}-r_{21}\rho_{22}, \quad (9)$$

$$d\rho_{33}/dt=2\,\mathrm{Im}[e_2^*\sigma_{31}]+2\,\mathrm{Im}[e_3^*\sigma_{32}]+r_{13}\rho_{11}-(r_{31}+r_{32})\rho_{33},$$

where r_{ik} are relaxation rates of transitions $i\rightarrow k$, r_{13} is the rate of pumping from level 1 to level 3. In semiconductors, this is valid for bipolar injection with equal injection rates of electrons to level 3 and holes to level 1. The index j is again omitted in Eqs. (9).

For QW lasers, the rates of spontaneous interband and intersubband transitions and injection pumping are usually much slower than the rate of intrasubband scattering that tends to bring the subband populations to quasithermal equilibrium. Therefore, we can represent the phenomenological rate equations for populations as follows [21]:

$$d\rho_{11}/dt+r_1(\rho_{11}-\overline{\rho}_{11})=-2\,\mathrm{Im}[e_1^*\sigma_{21}]-2\,\mathrm{Im}[e_2^*\sigma_{31}],$$

$$d\rho_{22}/dt+r_2(\rho_{22}-\overline{\rho}_{22})=2\,\mathrm{Im}[e_1^*\sigma_{21}]-2\,\mathrm{Im}[e_3^*\sigma_{32}], \quad (10)$$

$$d\rho_{33}/dt+r_3(\rho_{33}-\overline{\rho}_{33})=2\,\mathrm{Im}[e_2^*\sigma_{31}]+2\,\mathrm{Im}[e_3^*\sigma_{32}].$$

Here, r_i, $i=1,2,3$ are the rates of intrasubband scattering, $\overline{\rho}_{ii}(\delta_j)$ are the distributions of populations supported by pumping in the absence of strong laser fields.

III. LOWER LADDER SCHEME: INFRARED GENERATION IN SEMICONDUCTOR LASERS

In this section we suppose that a strong optical-field E_1 is excited in the laser cavity at frequency ω_{c1} equal to the central frequency ω_{21} of $2\rightarrow1$ transition. As the most general case, consider the instability of a weak bichromatic field E_2+E_3 in the presence of strong field E_1, see Fig. 1(b). When $d_2\ll d_{1,3}$ and $e_2\simeq0$, the problem is reduced to the lower ladder scheme in Fig. 1(a). It will be shown that the case $d_1\simeq d_2$ is more favorable since the excitation threshold for a bichromatic field can be lower than for the monochromatic field.

This kind of scheme can be straightforwardly applied to the inversionless IR generation in semiconductor lasers using transitions between levels of dimensional quantization. In the simplest case, only three levels are involved in generation: one (lowest-lying) heavy-hole level 1, and two electron levels 2,3; see Fig. 2. Of course, this scheme also describes the situation when there are two hole levels and one electron level involved.

In semiconductor lasers, the strong optical-field E_1 is generated at the interband recombination transition between

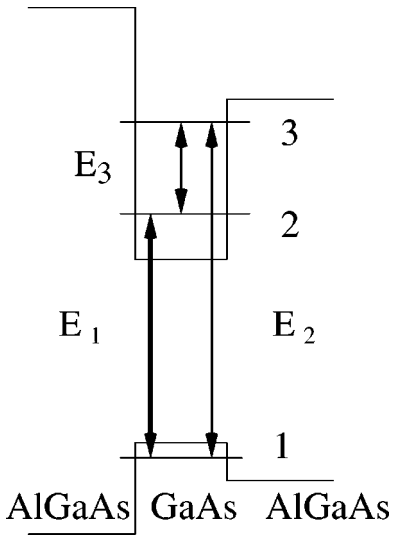

FIG. 2. Implementation of the lower ladder scheme in a quantum well. Asymmetry of the well is needed in order to make all transitions allowed. The shown example corresponds to a 60 Å GaAs quantum well surrounded by $Al_{0.35}Ga_{0.65}As$ and $Al_{0.28}Ga_{0.78}As$ barriers. Weak infrared field E_3 at $\lambda=8$ μm (or bichromatic field E_2+E_3) is excited on the transition between two levels of dimensional quantization. Strong driving field E_1 at $\lambda=0.82$ μm is provided by simultaneous lasing on the interband transition between electron and hole ground states.

ground electron and hole states. With an increase of pumping current, the population of the excited electron level 3 grows. When it exceeds some threshold value, which is still much less than the population of level 2, oscillations of the weak IR field E_3 and polarization σ_{32} at the low-frequency intersubband transition start growing exponentially. The instability is driven by the mixing of the optical-field e_1 and polarization σ_{31} [second term on the right-hand side of Eq. (7)], where the latter is excited by a two-photon term: $\sigma_{31} \propto e_3\sigma_{21} \propto e_3 e_1 n_{12}$.

Another way of generating the field E_3 is by instability of the bichromatic field E_2+E_3 that develops due to parametric coupling between partial components E_2 and E_3 mediated by a strong optical-field E_1. This can happen for *lower* pumping rates than the excitation of a single monochromatic mode E_3, and even without population inversion between states 3 and 1. In this case, we need all three transitions to be allowed by selection rules. In a QW, this will generally require using asymmetric structures, e.g., a rectangular well with different barrier heights as shown in Fig. 2. Symmetric QW's can be employed in some special cases, e.g., in the case of a strong coupling between different subbands of heavy and light holes. In self-assembled InAs/GaAs QD's, the three-level scheme can be easily realized with all three transitions allowed [22].

Another requirement for the efficient IR generation by means of the bichromatic excitation is the phase matching between the IR mode and the polarization wave created due to the difference-frequency mixing of interband optical fields E_1 and E_2. This requires a special wave guide design since refractive indices of bulk semiconductor materials for optical (near-IR) and mid/far-IR frequencies are different. The experimental work is in progress in this direction, and this issue will be discussed in detail elsewhere.

To find the generation threshold for the bichromatic field e_2, e_3, we search for the instability of small-amplitude self-consistent oscillations e_2, e_3, σ_{31}, $\sigma_{32} \propto \exp(-i\omega t)$, assuming for simplicity $\omega_{c1}=\omega_{21}$. The brief outline of this procedure is as follows. After adiabatic elimination of polarizations (see below) we are left with the linear system of the differential equations for two variables $e_2(t)$ and $e_3(t)$ with time-independent coefficients. The instability of the steady-state $e_2=e_3=0$ is sought in a standard way, by applying a temporal Laplace transformation with a complex parameter ω. This is of course equivalent to looking for the solution proportional to $\exp(-i\omega t)$. This results in a set of algebraic Eqs. (14), (15) with respect to Laplace transforms $\bar{e}_2(\omega)$, $\bar{e}_3(\omega)$. To have a nontrivial solution, the determinant of coefficients of this system should be equal to zero. The last requirement yields the characteristic, or dispersion Eq. (16) with respect to the complex parameter ω. We have to find eigenvalues of ω (roots of dispersion equation). The corresponding eigenvectors of Eqs. (14) and (15) are called normal modes. The stability of the normal modes is defined by the location of eigenvalues on the complex plane $[\mathrm{Re}(\omega), \mathrm{Im}(\omega)]$. Namely, the given mode is unstable if corresponding $\mathrm{Im}(\omega)>0$.

Since the resulting growth rate $\mathrm{Im}(\omega)$ turns out to be much smaller than the relaxation rates of polarizations, the adiabatic elimination of polarizations is justified. Then, the expressions for the polarizations σ_{ik} in a linear approximation with respect to e_2, e_3 take the form

$$\sigma_{21}=-ie_1 n_{21}/\Gamma_{21}, \tag{11}$$

$$\sigma_{31}=\frac{ie_2(n_{13}+|e_1|^2 n_{21}/(\Gamma_{32}\Gamma_{21}^*))+e_3 e_1(n_{21}/\Gamma_{21}+n_{23}/\Gamma_{32})}{\Gamma_{31}+|e_1|^2/\Gamma_{32}}, \tag{12}$$

$$\sigma_{32}=\frac{ie_3(n_{23}-|e_1|^2 n_{21}/(\Gamma_{31}\Gamma_{21}))+e_2 e_1^*(n_{13}/\Gamma_{31}+n_{21}/\Gamma_{21}^*)}{\Gamma_{32}+|e_1|^2/\Gamma_{31}}. \tag{13}$$

After substituting the above expressions into Eqs. (3),(4) and assuming that $e_2, e_3=\bar{e}_{2,3}\exp(-i\omega t)$, we obtain a set of two algebraic equations for the field amplitudes $\bar{e}_2$, $\bar{e}_3$:

$$(\omega-\Delta_2+2\pi\omega_{31}\chi_{22}+i\kappa_2)\bar{e}_2+2\pi\omega_{31}\chi_{23}\bar{e}_3=0, \quad (14)$$

$$-2\pi\omega_{32}\chi_{32}\bar{e}_2+(\omega-\Delta_3+2\pi\omega_{32}\chi_{33}+i\kappa_3)\bar{e}_3=0, \quad (15)$$

where $\Delta_2=\omega_{31}-\omega_{c2}$, $\Delta_3=\omega_{32}-\omega_{c3}$.

Here we introduced a set of linear (with respect to $E_{2,3}$) susceptibilities that describe the responses of polarizations P_{31}, P_{32} on the transitions $3\to1$ and $3\to2$ on the weak fields E_2, E_3, and are defined by

$$P_{31}=\chi_{22}E_2+\chi_{23}E_3,$$

$$P_{32}=\chi_{33}E_3+\chi_{32}E_2.$$

The expressions for χ_{ik} follow immediately from Eqs. (11)–(13):

$$\chi_{22}=\sum_j \frac{i\eta_2^2[n_{13}+|e_1|^2 n_{21}/(\Gamma_{32}\Gamma_{21}^*)]}{\omega_{31}(\Gamma_{31}+|e_1|^2/\Gamma_{32})},$$

$$\chi_{33}=\sum_j \frac{i\eta_3^2[n_{23}-|e_1|^2 n_{21}/(\Gamma_{31}\Gamma_{21})]}{\omega_{32}(\Gamma_{32}+|e_1|^2/\Gamma_{31})},$$

$$\chi_{32}=\sum_j \frac{\eta_3^2 e_1^*(n_{21}/\Gamma_{21}^*-n_{13}/\Gamma_{31})}{\omega_{32}(\Gamma_{32}+|e_1|^2/\Gamma_{31})},$$

$$\chi_{23}=\sum_j \frac{\eta_2^2 e_1(n_{21}/\Gamma_{21}+n_{23}/\Gamma_{32})}{\omega_{31}(\Gamma_{31}+|e_1|^2/\Gamma_{32})},$$

where

$$\eta_i^2=\frac{\omega_{ci}d_i^2 NG_i}{\hbar n_i^2}, \quad i=1,2,3$$

are coupling coefficients between the field and polarization, G_i are the optical confinement factors that measure the overlap of the mode-field distributions with an active region, and all other notation is the same as in Sec. II.

Equations (14) and (15) have a nonzero solution if their determinant is equal to zero. This requirement gives us the dispersion relation for the complex frequency ω as a function of detunings $\Delta_{2,3}$:

$$(\omega-\Delta_2+2\pi\omega_{31}\chi_{22}+i\kappa_2)(\omega-\Delta_3+2\pi\omega_{32}\chi_{33}+i\kappa_3)+4\pi^2\omega_{31}\omega_{32}\chi_{32}\chi_{23}=0. \quad (16)$$

The real parts of the terms $\mathcal{G}_2\equiv i2\pi\omega_{31}\chi_{22}-\kappa_2$, $\mathcal{G}_3\equiv i2\pi\omega_{32}\chi_{33}-\kappa_3$ in Eq. (16) represent growth rates of the partial modes e_3, e_2, respectively. For example, when the transition $3\to1$ is forbidden and $e_2\simeq0$, the inequality Re $\mathcal{G}_3>0$ is the excitation condition for the IR field e_3 in the presence of a strong driving field e_1. When both Rabi frequencies e_3 and e_2 are comparable, the dynamics is richer due to the interaction of two partial modes, and contains more possibilities for the IR generation of the field E_3.

The condition for the instability of the bichromatic field is

$$\mathrm{Im}\,\omega>0. \quad (17)$$

The maximum growth rate is achieved at the line center, $\Delta_2=\Delta_3=0$.

Note that the population differences and the field e_1 are not free parameters, and should be found from the requirement of steady-state generation on the transition $2\to1$. For example, when the model (10) for populations in QW subbands is accepted, we have

$$n_{21}=\bar{n}_{21}/(1+4a_1^2),$$

$$n_{13}=\bar{n}_{13}+2a_1^2\bar{n}_{21}/(1+4a_1^2), \quad (18)$$

$$n_{23}=\bar{n}_{13}+\bar{n}_{21}(1+2a_1^2)/(1+4a_1^2),$$

where

$$a_1^2=\gamma_{21}|e_1|^2/(r_1|\Gamma_{21}|^2),$$

the quantities $\bar{n}_{ik}$ are the population differences supported by pumping in the absence of generation. Here we again dropped the index j. The field intensity can be obtained from the equation

$$\kappa_1=\gamma_{21}\eta_1^2\sum_j \frac{\bar{n}_{21}}{\gamma_{21}^2+\delta_j^2+4\gamma_{21}|e_1|^2/r_1}. \quad (19)$$

When the inhomogeneously broadened line has the Lorentzian shape of width u_{21}, Eq. (19) yields

$$\frac{4|e_1|^2}{r_1\gamma_{21}}=\frac{u_{21}}{2\gamma_{21}}\left[-1+\left(1+\frac{4\eta_1^2\gamma_{21}\bar{n}_{21}}{\kappa_1 u_{21}^2}\right)^{1/2}\right]^2-1. \quad (20)$$

When the inhomogeneous broadening is negligible, we obtain

$$n_{21}=\frac{\gamma_{21}\kappa_1}{\eta_1^2}, \quad \frac{4|e_1|^2}{r_1\gamma_{21}}=\frac{\bar{n}_{21}}{n_{21}}-1. \quad (21)$$

For the model described by Eqs. (9), populations have the same functional dependence on δ_j and $|e_1|^2$ as in the model (10), with r_i and $\bar{n}_{ii}$ being rather lengthy functions of relaxation and pumping rates r_{ik}. In particular, expressions (19)–(21) remain valid after the substitution

$$\bar{n}_{21}=\frac{r_{13}-r_{21}-r_{31}p}{p(r_{21}-r_{31})+r_{21}+r_{13}},$$

$$r_1=2\frac{p(r_{21}-r_{31})+r_{21}+r_{13}}{2+p},$$

where the normalized pumping rate $p=r_{13}/(r_{32}+r_{31})$.

It is worth noting that for $r_{32}>r_{21}$ and in the absence of generation on the drive transition, the population inversion on the operating 3-2 transition cannot be achieved at *any* incoherent pumping rate since $\bar{n}_{23}\propto r_{32}-r_{21}$. When the drive-field intensity becomes much greater than saturation

value, the 3-2 transition can be inverted, in principle, if $p>1$. However, for semiconductor lasers this requires field intensities greater than the degradation threshold; see below.

A. Homogeneous broadening

The intersubband transition can be homogeneously broadened in high-quality structures. The main reasons for inhomogeneous broadening are growth defects leading to interface roughness, fluctuations in the well widths and barrier heights, and size fluctuations in the case of quantum-dot lasers. Recent progress in molecular-beam epitaxy technology allows one to routinely grow quantum-well structures with purely homogeneous broadening of the intersubband transition even at room temperature [23].

In the case of homogeneous broadening, the requirement (17) yields at the line center:

$$|e_1|^2-\frac{\gamma_{21}^2 n_{23} n_{13}}{n_{21}^2}>K\left(|e_1|^2+\frac{\gamma_{21}\gamma_{32}n_{13}}{n_{21}}\right)+K_2\left(-|e_1|^2+\frac{\gamma_{21}\gamma_{31}n_{23}}{n_{21}}\right)+KK_2(\gamma_{31}\gamma_{32}+|e_1|^2), \tag{22}$$

where

$$K=\frac{\kappa_3}{\kappa_1}\frac{\eta_1^2}{\eta_3^2}, \quad K_2=\frac{\kappa_2}{\kappa_1}\frac{\eta_1^2}{\eta_2^2}. \tag{23}$$

For vanishing cavity losses κ_3, $\kappa_2=0$ on the $3\rightarrow 2$ and $3\rightarrow 1$ transitions, we recover from Eq. (22) the known result [11]:

$$|\sigma_{21}|^2=|e_1|^2 n_{21}^2/\gamma_{21}^2>n_{13}n_{23}. \tag{24}$$

Note that when the transition $3\rightarrow 1$ is forbidden and $e_2\simeq 0$, the excitation condition at the line center takes the form

$$n_{23}<|e_1|^2 n_{21}/(\gamma_{21}\gamma_{31}), \tag{25}$$

which requires a higher pumping rate to the level 3, as compared with excitation of the bichromatic field. Indeed, it is easy to express Eq. (25) as

$$\frac{|e_1|^2}{\gamma_{31}\gamma_{21}}[pr_{32}-r_{21}-2\gamma_{31}(1-p)]-p(r_{32}-r_{21})>0, \tag{26}$$

from which we obtain that the threshold pumping rate p decreases steadily with increasing drive intensity and in the limit $|e_1|^2/(\gamma_{31}\gamma_{21})\gg 1$ approaches $p\simeq 0.6$.

At the same time, the excitation threshold for the bichromatic field and the required intensity of the driving field are much lower; see Fig. 3. It shows the driving-field dependence of the normalized pumping rate $p=r_{13}/r_{32}$, which is needed to achieve the excitation threshold Im $\omega=0$ for a bichromatic field. The horizontal axis shows the driving-field intensity $I_1=4|e_1|^2/(r_1\gamma_{21})$ normalized by the saturation intensity $|e_1|^2_{\rm sat}=r_1\gamma_{21}/4$ for the $2\rightarrow 1$ transition. The curve in Fig. 3 reaches its minimum $r_{13}\simeq 0.15(r_{32}+r_{31})$ at $|e_1|^2/|e_1|^2_{\rm sat}\simeq 0.2$, when the population density ρ_{33} at the level 3 is only 0.01 of the total electron density, while $\rho_{22}\simeq 0.9$. It can be shown that the minimum value of incoherent pumping rate scales as $p_{\rm min}\sim(r_{21}/r_{32})^{1/3}$ and is reached for the driving fields below saturation value.

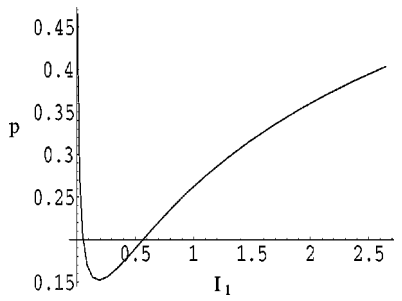

FIG. 3. The normalized pumping rate $p=r_{13}/r_{32}$ required to achieve the excitation threshold, as a function of the driving field intensity $I=|e_1|^2/|e_1|^2_{\rm sat}$ normalized by the saturation intensity $|e_1|^2_{\rm sat}=r_1\gamma_{21}/4$ for the $2\rightarrow 1$ transition. The curve is plotted for the bichromatic scheme in Fig. 1(b).

Now let us take into account nonresonant losses κ_3, κ_2. For a single-monochromatic field e_3, the excitation condition takes the form

$$K_{\rm th}\equiv\frac{|e_1|^2-\gamma_{21}\gamma_{31}n_{23}/n_{21}}{\gamma_{31}\gamma_{32}+|e_1|^2}>K. \tag{27}$$

This condition is illustrated in Fig. 4, which shows the factor $K_{\rm th}$ as the function of pumping parameter $p=r_{13}/r_{32}$ for $n_{21}=\kappa_1\gamma_{21}/\eta_1^2=0.05$, which roughly corresponds to the driving field intensity $|e_1|^2/|e_1|^2_{\rm sat}\simeq 18$. As is clear from Eq. (27), this curve determines, for given p, the value of nonresonant losses K corresponding to excitation threshold. Con-

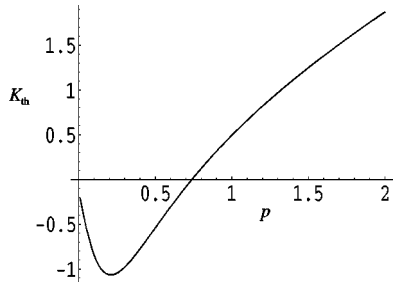

FIG. 4. $K_{\rm th}$, the left-hand side of the excitation condition (27) for the monochromatic field E_3 as a function of pumping rate $p=r_{13}/r_{32}$, showing the value of nonresonant losses K corresponding to the excitation threshold.

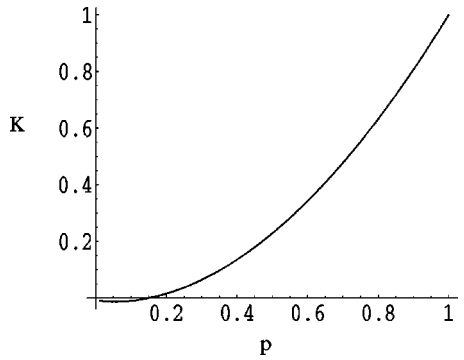

FIG. 5. $K_{\rm th}$, the left-hand side of the excitation condition (28) for the bichromatic normal wave E_2+E_3 as a function of pumping rate $p=r_{13}/r_{32}$, showing the value of nonresonant losses K corresponding to the excitation threshold.

versely, for given losses K we can find from Fig. 4 the minimum pumping required to surpass the threshold.

For the bichromatic field, the excitation condition is given by inequality (22). If $K \gg K_2$ and the terms containing K_2 are neglected, Eq. (22) can be rewritten as

$$K_{\rm th} \equiv \frac{|e_1|^2 - \gamma_{21}^2 n_{23} n_{13}/n_{21}^2}{|e_1|^2 + \gamma_{32}\gamma_{21} n_{13}/n_{21}} > K. \qquad (28)$$

Figure 5 shows the left-hand side of this inequality as the function of the pumping parameter $p=r_{13}/r_{32}$ for the driving-field intensity $|e_1|^2/|e_1|^2_{\rm sat} \simeq 0.2$. For these values of parameters, the partial growth rates Re $\mathcal{G}_3$, Re $\mathcal{G}_2$ are negative, and the partial modes e_3 and e_2 decay for any p. Therefore, the instability develops entirely due to parametric coupling of two weak components of the bichromatic field, mediated by coherence σ_{21} created by a strong driving field e_1.

As is seen from comparing Figs. 4 and 5, at the given level of nonresonant losses K the excitation of a bichromatic field requires substantially lower pumping power and driving-field intensity than the excitation of a single e_3 field. The value of the driving-field intensity is only about 0.2 of the saturation value, while the excitation of a monochromatic e_3 mode requires $|e_1|^2/|e_1|^2_{\rm sat} \sim 10$. However, this bichromatic mechanism of instability can be sensitive to the value of the parameter K_2 characterizing nonresonant losses on the $3 \rightarrow 1$ transition. This is illustrated in Fig. 6, which shows pumping parameter p at the excitation threshold as a function

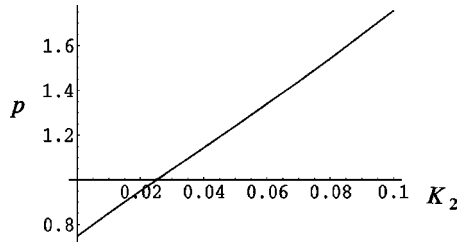

FIG. 6. The pumping rate $p=r_{13}/r_{32}$ at the excitation threshold of the bichromatic field as a function of normalized nonresonant losses K_2.

of K_2 for $K=0.5$, $n_{21}=2/3$, when the driving-field intensity $|e_1|^2/|e_1|^2_{\rm sat} \sim 0.4$. At the same time, for $n_{21}=0.05$, when $|e_1|^2/|e_1|^2_{\rm sat} \sim 18$, the threshold pumping for a bichromatic field practically does not depend on the value of K_2. Apparently, in this region of parameters the instability is due to the excitation of partial e_3 mode that has the growth rate $\mathcal{G}$ independent on K_2.

B. Inhomogeneous broadening

In the general case of inhomogeneous broadening, it is difficult to derive transparent excitation conditions such as Eqs. (24)–(28), and we provide a numerical analysis. To minimize the number of free parameters, let us adopt the QW-like model (10) for relaxation of populations and assume that all rates r_i and γ_{ik} of incoherent relaxation of populations $n_i(\delta_j)$ and polarizations $\sigma_{ik}(\delta_j)$ are equal to the same value γ. This can be a reasonable approximation for QW lasers, where the dephasing of excited polarization and the relaxation of particle distributions are defined by the same process of intrasubband scattering with typical rate $\gamma \sim 3-10$ meV (timescale $\sim 70-200$ fs). More precisely, the relaxation rates are of course energy dependent. The initial relaxation of injected hot carriers occurs with timescale $\lesssim 10$ fs. The relaxation times in Eqs. (10) are related to partially degenerate carriers close to the spectral positions of laser modes. These relaxation times describe the filling of spectral holes burned by laser field and should be substantially longer due to Fermi degeneracy. Note that the injection of carriers that supports quasi-Fermi levels of carriers occurs on a much longer timescale. The relevant parameters that characterize the efficiency of generation schemes are the populations $\overline{n_i}$ supported by pumping (in the absence of generation) and the intensity of a driving-field $|e_1|^2$ required for excitation of IR radiation e_3. The value of $|e_1|^2$ can be changed independently on $\overline{n_i}$ by, e.g., varying cavity losses. Of course, for a given heterostructure, cavity, and wave guide, both parameters are defined by the pumping rate.

The saturation intensity for the above values of γ is of the order of 10 MW/cm^2. This is already close to the degradation threshold of QW lasers in the cw regime. Therefore, inequality $|e_1| \gg \gamma$ can be realized in QW lasers only in the pulsed regime. We assume, for simplicity, that the inhomogeneous widths $u_{21}=u_{32}=u \gg \gamma, |e_1|$. If the distance from the spectral position of a laser mode E_1 to the edges of the inhomogeneous profile is much greater than the power-broadened homogeneous linewidth $\sqrt{\gamma^2+4|e_1|^2}$, the precise shape and asymmetry of the inhomogeneously broadened line is not important for the excitation threshold, and we can replace it by Lorentzian.

Let us characterize the threshold conditions for the excitation of the weak-field e_3 or e_2+e_3 by a ratio of pumping-supported population differences $b=\overline{n_{31}}/\overline{n_{21}}$, calculated in the absence of generation of a field e_1 at the instability threshold Im $\omega=0$. When $b<0$, there is no inversion both on $3 \rightarrow 1$ and $3 \rightarrow 2$ transitions. For $0<b<1$, there is an inversion at $3 \rightarrow 1$ transition, but no inversion on $3 \rightarrow 2$ transition. We show below that inversionless lasing of the IR

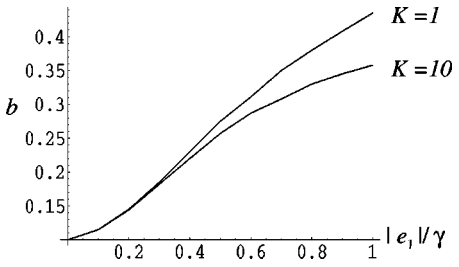

FIG. 7. Pumping-supported population difference $b=\bar{n}_{31}/\bar{n}_{21}$ as a function of the driving field strength $|e_1|/\gamma$. The parameters K and K_2 characterizing nonresonant losses were chosen to be $K=1$, $K_2=0.1$ (upper curve), and $K=10$, $K_2=0.1$ (lower curve).

field under the condition of strong inhomogeneous broadening $|e_1| \lesssim \gamma \ll u$ is possible when $0<b=\bar{n}_{31}/\bar{n}_{21} \ll 1$, i.e., when there is population inversion on both 2-1 and 3-1 optical transitions, but still no inversion on the intersubband 3-2 transition. This may seem to be not very exciting. However, the most important point is that the pumping threshold can be several times lower as compared to the pumping rate required to provide population inversion directly on the intersubband transition 3-2. One should keep in mind that even the reduction of the injection current by a factor of two is crucial for the intersubband IR lasers since it may lead to a transition from liquid-nitrogen to room-temperature operation.

Figure 7 shows the parameter $b=\bar{n}_{31}/\bar{n}_{21}$ required to achieve the excitation threshold Im $\omega=0$ as a function of the driving-field $|e_1|/\gamma$. The parameters K and K_2 characterizing nonresonant losses were chosen to be $K=1$, $K_2=0.1$ (upper curve), and $K=10$, $K_2=0.1$ (lower curve). The function $b(|e_1|/\gamma)$ turns out to be practically independent of K, but sensitive to the value of K_2. For given $|e_1|$, it behaves approximately as $b \sim 0.01+K_2$. This suggests that the excitation of the bichromatic field in this region of parameters is due to instability of the partial e_2 mode that develops only when there is population inversion on the 3-1 transition. This is illustrated in Fig. 8, which shows the growth rate Re $\mathcal{G}_2$ for the partial e_2 wave (upper curve) and the growth rate Im ω for the bichromatic field (lower curve) as functions of $|e_1|/\gamma$ for $b=0.3$ and $K=1$, $K_2=0.2$. The growth rates are normalized by $\eta_3^2\kappa_1/\eta_1^2$. Both curves have qualitatively similar be-

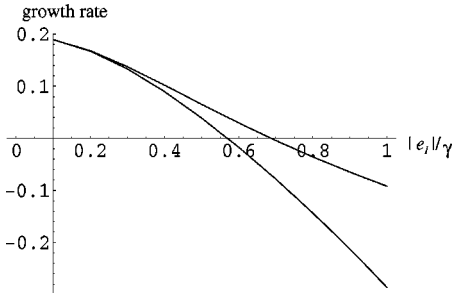

FIG. 8. The growth rates for the partial E_2 wave (upper curve) and the bichromatic field (lower curve) as functions of $|e_1|/\gamma$ for $b=0.3$ and $K=1$, $K_2=0.2$. The growth rates are normalized by $\eta_3^2\kappa_1/\eta_1^2$.

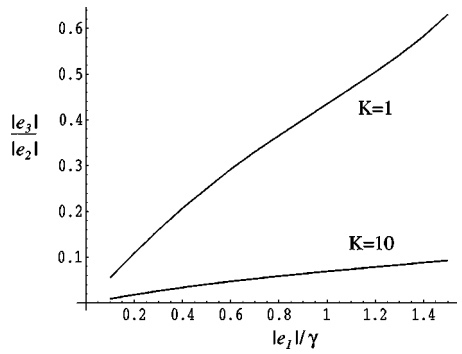

FIG. 9. The ratio $|e_3|/|e_2|$ of two components in the bichromatic normal wave as a function of the driving-field strength $|e_1|/\gamma$ for two values of K: $K=1$ (upper curve) and $K=10$ (lower curve).

havior. Thus, under the conditions of strong inhomogeneous broadening it is the partial wave e_2 that helps to involve the field e_3 in the inversionless generation. The price one should pay for such generosity is obvious: the mixing ratio of the field e_3 in the bichromatic normal wave is rather small. Figure 9 shows this ratio $|e_3|/|e_2|$ as a function of $|e_1|/\gamma$ for two values of K: $K=1$ (upper curve) and $K=10$ (lower curve). With increasing nonresonant losses κ_3, the ratio $|e_3|/|e_2|$ decreases as $1/K$. It is clear that for small values of $|e_1|$, optimal for pumping, the bichromatic wave consists mainly of the field e_2. Of course, the precise numbers should change at the nonlinear stage, when the exponential growth of both fields is saturated, but the general tendency of a small ratio $|e_3|/|e_2|$ is likely to be preserved. As is clear from Figs. 8 and 9, the optimal choice of parameters is determined by the tradeoff between the requirements of a low pumping rate and the high efficiency of the IR generation. It is straightforward to find stationary field intensities in the case when two or three fields are simultaneously generated. To do this, we have to resolve Eqs. (5)–(7) with respect to steady-state polarizations σ_{ik} as functions of detunings and population differences, to find populations from Eqs. (9) or (10), and to substitute the resulting expressions for polarizations to field Eqs. (2)–(4). This analysis, along with the study of a nonlinear regime of IR generation by two strong optical fields, is done elsewhere [20].

IV. UPPER LEVEL LADDER SCHEME: APPLICATION TO HIGH-FREQUENCY LASERS

In this section we consider excitation of a weak-field E_1 resonant with a $2\rightarrow1$ transition, when the strong lasing field E_3 is generated on the transition $3\rightarrow2$; see Fig. 1(b). With respect to the field E_3 this is a standard four-level laser scheme in which the decay of the lower-laser state 2 to the ground-state 1 occurs much faster than the decay of the upper-laser state 3: $r_{21} \gg r_{32}$. We show below that a sufficiently strong driving-field E_3 gives rise to excitation of the field E_1 under the conditions $\rho_{22} \ll \rho_{11}$ and $\rho_{33} \ll \rho_{11}$ typical for the four-level scheme. This means that inversionless generation on the fast-decaying 2-1 transition is possible at low rates of incoherent pumping $r_{13} \ll r_{21}$. This should be compared with the pumping rate $r_{13} > r_{21}(1+r_{31}/r_{32})$ required to

provide population inversion on the 2-1 transition.

A natural application of the proposed scheme is UV and soft x-ray generation in gas lasers, especially employing hydrogen, helium, hydrogenlike, and heliumlike ions and some inert-gas ions. For example, in hydrogen, the $2p \rightarrow 1s$ transition at 121 nm corresponds to $2 \rightarrow 1$ transition in Fig. 1(c), while the $3s$ state can be used as level 3 in our scheme. The transition $3s \rightarrow 2p$ at wavelength 656 nm occurs with radiative lifetime of 159 ns, while the $2p$ state decays to the ground $1s$ state in 1.6 ns. In helium, the state $2p\ ^1P_1$ can be used as the level 2 of our scheme. It decays radiatively to the ground state in 0.6 ns emitting soft x-ray radiation at 58.4 nm. Level 3 corresponds to the $3s\ 1S_0$ state that decays to the $2p$ state in 54 ns, emitting radiation at 728 nm. In the well-known Ar^+ laser, generation of the driving field at $\lambda = 488$ or 514 nm occurs on the $4p \rightarrow 4s$ transition having a decay time of 10 ns. Relaxation from the $4s$ state to the ground $3p^5$ state occurs in 0.3 ns. This makes possible an inversionless generation of $\lambda = 72$ nm radiation on the $4s \rightarrow 3p^5$ transition. In all of the above examples, $r_{32}/r_{21} \sim 0.01$.

Actually, there are many candidates for high-frequency generation using our scheme that have a favorable ratio of relaxation times and convenient visible-range wavelengths for the driving field. The main criteria of choice are convenience of pumping and minimization of negative effects of inhomogeneous broadening.

The relevant set of equations is Eqs. (5)–(9). Here, we assume that transition $3 \rightarrow 1$ is strongly forbidden and $e_2 = 0$. This is typically the case in gas lasers when the transitions 2-1 and 3-2 are allowed. After linearization with respect to the weak-field e_1, we obtain from Eqs. (5)–(7) the expressions for off-diagonal elements of the density matrix:

$$\sigma_{21} = \frac{ie_1[n_{12} - |e_3|^2 n_{32}/(\Gamma_{31}\Gamma_{32})]}{\Gamma_{21} + |e_3|^2/\Gamma_{31}}, \tag{29}$$

$$\sigma_{31} = -\frac{e_1 e_3 (n_{12}/\Gamma_{21} + n_{32}/\Gamma_{32})}{\Gamma_{31} + |e_3|^2/\Gamma_{21}}, \tag{30}$$

$$\sigma_{32} = -ie_3 n_{32}/\Gamma_{32}. \tag{31}$$

Here, all population differences and the driving-field intensity are easily derived from Eqs. (9) together with a steady-state generation condition similar to Eq. (19):

$$\kappa_3 = \gamma_{32}\eta_3^2 \sum_j \frac{\bar{n}_{32}}{\gamma_{32}^2 + \delta_j^2 + 4\gamma_{32}|e_3|^2/r_3}, \tag{32}$$

where

$$n_{32} = \frac{\bar{n}_{32}}{1 + 4a_3^2},$$

$$n_{12} = \frac{\bar{n}_{12}}{1 + 4a_3^2} + \frac{4a_3^2(r_{21} - r_{13})}{(1 + 4a_3^2)(r_{21} + 2r_{13})},$$

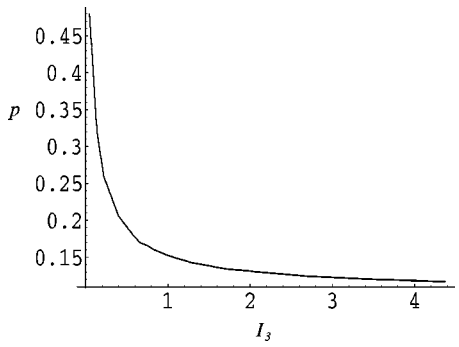

FIG. 10. The normalized pumping rate $p = r_{13}/r_{21}$ for the upper ladder scheme in Fig. 1(c), required to achieve the instability threshold, as a function of driving-field intensity $I_3 = 4|e_3|^2/(r_3\gamma_{32})$ measured in units of saturation intensity.

$$\bar{n}_{32} = \frac{r_{13}(r_{21} - r_{32})}{r_{32}r_{13} + r_{21}(r_{32} + r_{13})},$$

$$\bar{n}_{12} = \frac{r_{32}(r_{21} - r_{13})}{r_{32}r_{13} + r_{21}(r_{32} + r_{13})},$$

$$a_3^2 = |e_3|^2\gamma_{32}/(r_3|\Gamma_{32}|^2),$$

$$r_3 = 2\frac{r_{32}r_{13} + r_{21}(r_{32} + r_{13})}{r_{21} + 2r_{13}}.$$

The maximum growth rate of small-amplitude oscillations of field e_1 and polarization σ_{21} is given by

$$\mathrm{Im}\,\omega \simeq -\mathrm{Re}\left[\eta_1^2 \sum_j \sigma_{21}/(ie_1)\right] - \kappa_1. \tag{33}$$

The excitation condition has the form $\mathrm{Im}\,\omega > 0$. For homogeneous broadening, at zero detuning, and in the absence of nonresonant losses $\kappa_1 = 0$, this is equivalent to

$$|e_3|^2 n_{32} > \gamma_{31}\gamma_{32}n_{12},$$

where $n_{32} = \gamma_{32}\kappa_3/\eta_3^2$, $|e_3|^2 = (r_3\gamma_{32}/4)(\bar{n}_{32}/n_{32} - 1)$. When $n_{32} \ll \bar{n}_{32}$ (the driving field saturates the 3-2 transition), the latter inequality gives simply

$$r_{13} \gtrsim \sqrt{r_{21}r_{32}}. \tag{34}$$

Since $r_{32} \ll r_{21}$ the excitation of the field e_1 is possible when $r_{13} \ll r_{21}$ and $\rho_{22} \ll \rho_{11}$. This is illustrated in Fig. 10, where the normalized pumping parameter $p = r_{13}/r_{21}$, evaluated at the instability threshold, is plotted as a function of driving-field intensity $I_3 = 4|e_3|^2/(r_3\gamma_{21})$ measured in units of saturation intensity. Here we have taken $r_{32} = 0.01r_{21}$ that corresponds to a real situation in the examples below. One can see that the threshold incoherent pump is an order of magnitude lower than the one required to produce inversion; see the scaling (34). Note the absence of long-lived coherences in

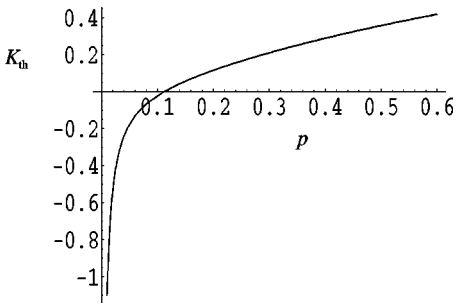

FIG. 11. The left-hand side of inequality (35) as a function of pumping parameter $p=r_{13}/r_{21}$ for $n_{32}=0.1$. This curve determines the value of normalized nonresonant losses K_1 corresponding to the excitation threshold.

the system. Similarly to lower ladder scheme, all relaxation rates of polarizations γ_{ik} contain large factors r_{21}, r_{13} or both.

When the nonresonant losses are taken into account, the inequality Im $\omega>0$ can be written in the following form, similar to Eq. (27):

$$K_{\mathrm{th}}\equiv\frac{|e_3|^2-\gamma_{31}\gamma_{32}n_{12}/n_{32}}{\gamma_{21}\gamma_{31}+|e_3|^2}>K_1\equiv\frac{\kappa_1}{\kappa_3}\frac{\eta_3^2}{\eta_1^2}. \qquad (35)$$

We illustrate this general requirement graphically. Figure 11 shows the left-hand side of this inequality as a function of pumping parameter $p=r_{13}/r_{21}$ for $n_{32}=0.1$, when the driving transition is already strongly saturated. Further decrease in the steady-state value of n_{32} (that is, increase in I_3) leads to little changes. According to Eq. (35), the curve in Fig. 11 determines, for given p, the value of nonresonant losses K_1 at the excitation threshold. Conversely, for given losses K_1, we can find from Fig. 11 the minimum pumping required to surpass the threshold.

Inhomogeneous broadening of the probe transition $2\rightarrow1$ seriously affects the excitation conditions. For the above examples, typical values of radiative broadening are hundreds of MHz, while Doppler broadening for room temperature is in the interval $1-10$ GHz. Numerical analysis for Doppler-broadened medium shows that the gain can be achieved without an increase in incoherent pump and driving-field intensity when the driving field is detuned from resonance by approximately the width of the inhomogeneously broadened line. In this case, Raman inversion is actually present in the system, which means $\bar{\rho}_{33}>\bar{\rho}_{11}\gg\bar{\rho}_{22}$. This conclusion is close to those obtained earlier for the folded schemes, and the advantages of a resonant ladder scheme in the case of large inhomogeneous broadening are lost.

Note, however, that for pumping by collisional excitation in a gas discharge, the UV transition is likely to be homogeneously broadened due to collisions with energetic electrons. In this case, the above analysis is directly applicable. If the broadening is mainly due to inelastic collisions and r_{21} remains much greater than r_{32}, the advantages of LWI in the resonant ladder scheme are preserved. Correct evaluation of effective relaxation and pumping rates requires solving a complicated set of kinetic rate equations for any specific experimental setup.

V. DISCUSSION

In this paper we have studied several three-level ladder-type schemes in which coherence-mediated inversionless generation becomes possible due to simultaneous lasing on the adjacent transition. The main outcome of our analysis is the possibility of exciting laser oscillations on transitions with very fast relaxation of population under conditions when supporting population inversion is difficult. In fact, the pumping threshold for amplification in the proposed schemes becomes much lower than needed for population inversion on the fast decaying transition since it is determined by the requirement of laser generation on another, long-lived transition, which is much easier to satisfy. This advantage is especially pronounced in the case of homogeneous broadening, though it can remain in a weaker form even in the case of inhomogeneous broadening. Of course, such an advantage is not given for free. The price is an additional requirement to the system parameters: favorable ratio of nonresonant cavity losses, or phase matching in the case of bichromatic excitation.

We have studied the application of those kind of inversionless schemes to the infrared generation in semiconductor lasers, and considered the possibility of high-frequency lasing in gas lasers.

Our calculations demonstrate the possibility to achieve generation of coherent mid/far-IR emission on intersubband (interlevel) transitions in standard multiple QW or QD laser diodes of simple design. The prerequisite for this is simultaneous lasing on the interband transitions, which provides necessary drive fields. This mechanism does not require population inversion on the IR transition, and can operate under the conditions of ultrafast dephasing times typical for semiconductor lasers. The proposed scheme is quite insensitive to inevitably large nonresonant IR losses and seems to be viable in the far-infrared region where very few semiconductor sources exist.

In gas lasers, our results indicate the principal possibility of CW inversionless UV and soft x-ray lasing, with probable candidates including hydrogen, helium, hydrogenlike, and heliumlike ions and other inert-gas ions, under the condition of inversion-based optical lasing on the adjacent transition.

ACKNOWLEDGMENTS

We appreciate the support from the Texas Advanced Technology Program, the Office of Naval Research, High Energy Lasers Program of Department of the Defense, and the National Science Foundation.

[1] O. Kocharovskaya, Phys. Rep. **219**, 175 (1992); M. O. Scully and M. S. Zubairy, *Quantum Optics* (Cambridge University Press, Cambridge, 1997); J. Mompart and R. Corbalán, Quantum Semiclassic. Opt. **2**, R7 (2000).
[2] O. Kocharovskaya, R. Kolesov, and Yu. Rostovtsev, Phys. Rev. Lett. **82**, 3593 (1999).
[3] H. Schmidt, D. E. Nikonov, and K. L. Campman *et al.*, Laser Phys. **9**, 797 (1999).
[4] S. E. Harris, J. E. Field, and A. Imamoglu, Phys. Rev. Lett. **64**, 1107 (1990).
[5] M. O. Scully, Phys. Rev. Lett. **67**, 1855 (1991).
[6] V. Ahufinger, J. Mompart, and R. Corbalán, Phys. Rev. A **61**, 053 814 (2000).
[7] J. Mompart, R. Corbalán, and R. Vilaseca, Opt. Commun. **147**, 299 (1998).
[8] S. F. Yelin, M. D. Lukin, M. O. Scully, and P. Mandel, Phys. Rev. A **57**, 3858 (1998).
[9] V. Ahufinger, J. Mompart, and R. Corbalán, Phys. Rev. A **60**, 614 (1999).
[10] G. B. Prasad and G. S. Agarwal, Opt. Commun. **86**, 409 (1991).
[11] O. Kocharovskaya, P. Mandel, and Y. V. Radeonychev, Phys. Rev. A **45**, 1997 (1992).
[12] Y. Zhu, Opt. Commun. **105**, 253 (1993).
[13] R. F. Kazarinov and R. A. Suris, Sov. Phys. Semicond. **5**, 707 (1971).
[14] J. Singh, IEEE Photonics Technol. Lett. **8**, 488 (1996).
[15] L. E. Vorob'ev, D. A. Firsov, and V. A. Shalygin *et al.*, Tech. Phys. Lett. **24**, 590 (1998).
[16] *Semiconductor Lasers*, edited by E. Kapon (Academic Press, San Diego, 1999).
[17] *Intersubband Transitions in Quantum Wells: Physics and Devices*, edited by S. S. Li and Y.-K. Su (Kluwer, Boston, 1998).
[18] J. Faist, F. Capasso, and D. L. Sivko *et al.*, Science **264**, 553 (1994).
[19] F. Capasso, C. Gmachl, and A. Tredicucci *et al.*, Opt. Photonics News **10**, 33 (1999).
[20] A. A. Belyanin, F. Capasso, V. V. Kocharovsky, Vl. V. Kocharovsky, and M. O. Scully, Phys. Rev. A **63**, 053803 (2001).
[21] W. W. Chow and S. W. Koch, *Semiconductor-Laser Fundamentals* (Springer, Berlin, 1999).
[22] D. Bimberg, M. Grundmann, and N. N. Ledentsov, *Quantum Dot Heterostructures* (Wiley, New York, 1998).
[23] C. Sirtori, F. Capasso, D. L. Sivco, and A. Y. Cho, in *Intersubband Transitions in Quantum Wells: Physics and Device Applications II*, edited by H. C. Liu and F. Capasso (Academic Press, San Diego, 2000).